IRSTI 29.33.51 https://doi.org/10.26577/phst20261312

Nonlinear ultrafast laser processing of diamond surfaces for precision microfabrication

Y. White[1,2,*]

[1]University of Tennessee Space Institute, Tullahoma, USA
[2]Georgia Southern University, Swainsboro, USA
*e-mail: ywhite@georgiasouthern.edu

(*Received March 9, 2026; received in revised form April 8, 2026; accepted April 29, 2026)*

Ultrafast femtosecond laser processing provides a versatile platform for precision micro- and nanoscale modification of wide-bandgap materials such as diamond. In this work, the formation of microscale and submicron surface features on high-pressure high-temperature (HPHT) single-crystal diamond and chemical vapor deposition (CVD) diamond films is investigated using high-repetition-rate femtosecond laser pulses. Systematic experiments examined the influence of laser fluence, pulse energy, and spatial pulse overlap on ablation morphology, feature dimensions, and material response. Arrays of craters, microchannels, and reservoir structures were fabricated through localized ablation, demonstrating the capability of femtosecond laser processing for flexible surface microstructuring of diamond. Differences in ablation behavior between HPHT single-crystal and polycrystalline CVD diamond were analyzed in terms of structural and electronic properties. The depth of laser-machined features was determined using an acetate replication technique followed by scanning electron microscopy. Results show a strong dependence of feature geometry and ablation efficiency on processing conditions, with single-crystal diamond exhibiting deeper ablation and sharper features at comparable fluence. These findings highlight the role of nonlinear absorption and defect-mediated carrier dynamics in ultrafast laser–diamond interactions and suggest applications in diamond-based microfluidic devices, field-emission structures, and advanced electronic and photonic systems.

Keywords: femtosecond laser, laser ablation, diamond micromachining, laser nanomachining, ultrafast laser processing.

1. Introduction

Femtosecond laser micro- and nanomachining has emerged as a powerful technique for precision material processing due to its ability to deposit energy on timescales shorter than thermal diffusion within the lattice. As a result, energy confinement within the focal volume enables highly localized structural modification and material removal with minimal heat-affected zones and excellent spatial precision [1-4]. These characteristics make ultrafast laser processing particularly attractive for the fabrication of microscale and nanoscale structures in materials that are otherwise difficult to machine using conventional techniques. Recent studies have also investigated nanostructured materials and their optical properties in related contexts [5]. Wide range of materials including silicon nanostructures and carbon-based coating have been explored for technological applications [6].

Laser–matter interaction in wide-bandgap materials under ultrafast excitation is governed by strong-field ionization processes including multiphoton ionization, tunneling ionization described by Keldysh theory, and avalanche ionization driven by impact excitation [7-9]. Under sufficiently high intensities, these processes generate a dense electron plasma within the focal volume. Subsequent energy transfer from the excited electron system to the lattice can lead to a variety of material removal mechanisms, including Coulomb explosion, phase explosion, and rapid melting followed by vaporization [10, 4]. The relative contribution of these mechanisms depends on laser parameters such as pulse duration, fluence, and repetition rate, as well as on the electronic and structural properties of the material.

Diamond is a particularly compelling platform for ultrafast laser processing due to its exceptional physical and electronic properties. The growth and structural properties of diamond films produced by

CVD methods have been widely investigated [11]. Diamond exhibits the highest known thermal conductivity among bulk materials, extreme mechanical hardness, chemical inertness, and a wide electronic bandgap of approximately 5.5 eV [12]. These properties make diamond attractive for a wide range of advanced technologies, including high-power electronics, quantum photonics, radiation detectors, field-emission devices, and microfluidic systems [13-17].

In this work, we investigate femtosecond laser microstructuring of high-pressure high-temperature (HPHT) single-crystal diamond and plasma-enhanced chemical vapor deposition (PE-CVD) diamond films using high-repetition-rate femtosecond laser pulses. The influence of laser pulse energy, spatial overlap, and material structure on ablation morphology and feature formation is examined. Particular attention is given to the role of nonlinear absorption, incubation effects, and defect-mediated carrier dynamics in determining ablation efficiency and feature geometry.

2. Materials and methods

All surface features in this study were fabricated using a customized femtosecond laser ablation system. The system consisted of a diode-pumped, frequency-doubled Neodymium-doped Yttrium Orthovanadate ($Nd:YVO_4$) pump laser operating at 532 nm (Verdi V18, Coherent, Inc.), which pumped a Ti:Sapphire laser oscillator (Tsunami, Spectra-Physics, Inc.) and a regenerative amplifier (RegA 9000, Coherent, Inc.). The system produced ultrafast laser pulses at a central wavelength of 800 nm with a pulse duration of approximately 200 fs, pulse energies up to 4 μJ, and repetition rates as high as 250 kHz. The repetition rates could be controlled by an external transistor-transistor logic (TTL) pulse generator, directly connected to the amplifier.

The ablation time during experiments was controlled using an externally triggered mechanical shutter. Laser power was controlled by a neutral density filter placed into the beam path. The laser beam was focused onto the front surface of the samples using microscope objectives with numerical apertures (NA) of 0.85 and 0.90. Under these focusing conditions, the resulting focal spot diameter was approximately 0.55 μm. The objective was mounted on a stage with adjustable Z-positioning to allow precise focusing on the sample surface. The optical delivery system also enabled direct observation of the ablation region through a 10× eyepiece and a high-resolution digital camera.

Precise sample positioning was achieved using a piezoelectric nanopositioning stage (Mad City Labs, Inc.) that provided nanometer-scale resolution with a travel range of 200 μm in the X–Y directions and 100 μm in the Z direction. This stage was mounted on a larger-range X–Y microstage (McBain, Inc. precision stages equipped with Compumotor, Inc. stepper motors and National Instruments motor drivers). During the ablation process, the microstage remained fixed while the piezoelectric stage translated the sample at a scanning speed of approximately 11 μm/s to generate the desired micropatterns. Both positioning stages, as well as the mechanical shutter, were controlled through LabVIEW™ software. In addition to enabling the fabrication of individual features on a variety of materials, this configuration allowed precise alignment and placement of microstructures through software-controlled positioning with nanometer-scale accuracy. A He:Ne laser was introduced to the system for precise positioning purposes [18].

Figure 1 shows the experimental setup used for femtosecond laser ablation of diamond film surfaces [19]. Several corrective lenses were placed in the beam path to compensate for beam divergence and to match the beam size with the entrance aperture of the objective lens. The placement and optical configuration of these lenses were optimized using Zemax software in order to minimize spherical aberrations and preserve beam quality at the focus. This optical arrangement enabled high precision during laser ablation process and provided a flexible platform for performing parametric studies of laser ablation and micromachining across a broad range of operating conditions.

All experiments were performed in a controlled environment of a Class-1000 Clean Room. The samples were cleaned with acetone, methanol, and deionized water in an ultrasonic bath prior to laser ablation.

While the width of features, such as small holes, machined by femtosecond laser can be estimated from the numerical aperture of the focusing objective lens, the depth cannot be directly measured during laser machining. After ablation, sample surfaces were cleaned again, and replicated with cellulose-based acetate films. The acetate replication technique provides a cost-efficient, reliable, and nondestructive method for depth estimation. However, its fidelity depends on the aspect ratio of the replicated features. The reported depth values for high-aspect-ratio features should be considered as approximate lower bounds. Extended acetate film application and drying times were used to maximize filling, and the consistency of replica morphology in SEM images

supports adequate, though potentially not complete, penetration of the acetate material into these features This technique and the validity of depth estimation are described in detail in our previous work [18]. The replicas and diamond samples were then sputter-coated with carbon, platinum, or gold for conductivity and imaged with the Scanning Electron Microscope (SEM).

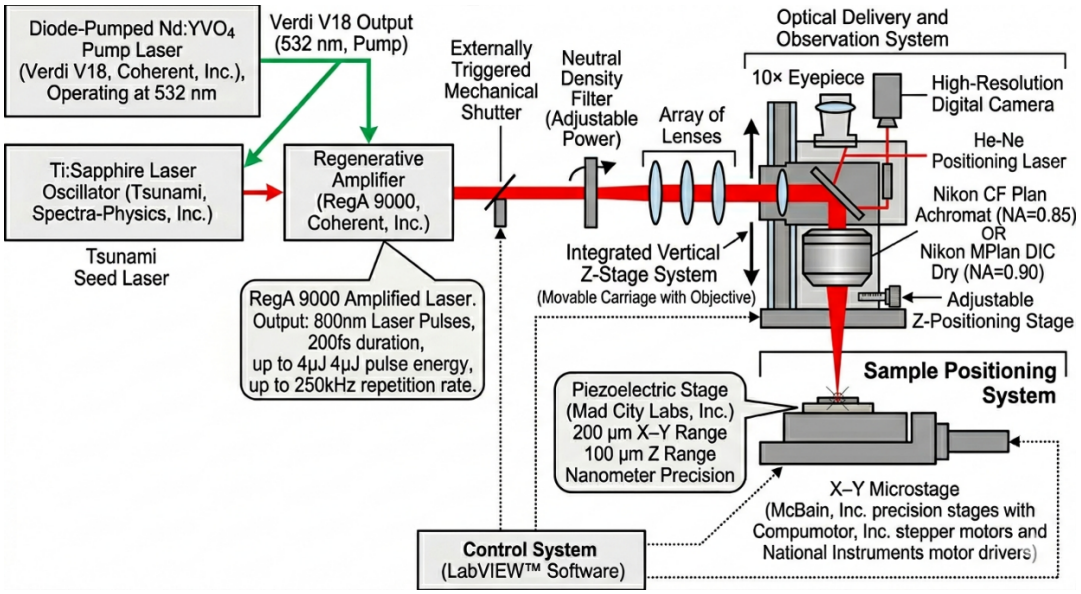

Figure 1. Schematic diagram of experimental setup for laser micro- and nanomachining.

In our experiments, we investigated two types of diamond materials: single-crystal diamond synthesized by the high-pressure high-temperature (HPHT) process, and polycrystalline diamond films produced by plasma-enhanced chemical vapor deposition (PECVD) [20, 21], a technique widely used for the fabrication of diamond-based and diamond-like carbon films for technological applications [22]. Ideal single-crystal diamond is largely transparent at the laser wavelength of 800 nm due to its wide electronic bandgap (~5.5 eV). Consequently, energy deposition under ultrafast irradiation occurs primarily through nonlinear absorption mechanisms such as multiphoton ionization and avalanche ionization [23]. In contrast, polycrystalline CVD diamond films often contain grain boundaries, defect states, and regions of sp^2-bonded carbon, which introduce sub-bandgap electronic states that can enhance linear and defect-assisted absorption at near-infrared wavelengths. These structural differences significantly influence carrier generation dynamics and energy coupling during femtosecond laser irradiation, thereby affecting the resulting ablation morphology and material removal efficiency [24-26].

At a repetition rate of 250 kHz, the interval between pulses is 4 μs. With the pulse width of 200 fs, the pulses are well-separated. Given the high thermal diffusivity of single-crystal diamond (~1200 mm^2/s), the thermal diffusion length within this interval far exceeds the sub-micron focal spot, ensuring that heat dissipates between successive pulses and that ablation proceeds in a predominantly non-thermal regime. In polycrystalline CVD diamond, grain boundaries and sp^2-bonded intergranular phases reduce the effective thermal conductivity; however, the thermal diffusion length during the 4 μs interpulse interval still substantially exceeds the focal volume dimensions. The clean feature morphology and minimal heat-affected zones observed in our SEM images (Figures 5, 6, 7 below) confirm that non-thermal ablation conditions are maintained for both materials at this repetition rate, consistent with recent studies of femtosecond laser structuring of diamond at comparable repetition rates [27, 28].

Although sp^2-bonded intergranular phases in CVD diamond enhance sub-bandgap optical absorption, these regions simultaneously function as carrier recombination centers and electron scattering sites that attenuate avalanche ionization buildup, thereby reducing the effective ablation efficiency relative to single-crystal diamond at comparable laser fluence [29, 30].

3. Results and discussion

In this work, diamond surface micropatterning is performed by localized material removal through femtosecond laser ablation at a precisely defined position on the surface. When an ultrafast pulse is tightly focused on the target material, the extremely high peak intensity within the focal volume initiates nonlinear absorption processes, including multiphoton ionization and avalanche ionization. These processes generate a population of free electrons that rapidly evolve into a dense microplasma near the surface. The subsequent expansion of this plasma results in the ejection of material from a highly confined region of the target. Because the energy deposition occurs on a timescale shorter than thermal diffusion in the lattice, the interaction proceeds largely in a nonthermal regime, often referred to as "cold ablation," which enables the fabrication of micron- and submicron-scale structures with minimal heat-affected zones and high edge fidelity [31-33].

A single ablation event typically produces an isolated crater or hole at the location of the laser focus. By translating the sample relative to the focal spot or by sequentially triggering pulses at predefined coordinates, multiple ablation sites can be arranged in desired patterns or arrays. Such arrays provide a convenient platform for evaluating the spatial precision and repeatability of the ablation process, as well as parametric studies of feature morphology, laser pulse energy, fluence, and repetition rate.

Figure 2(a) shows an array of ablation sites fabricated on the surface of a chemical vapor deposition (CVD) diamond film using a laser pulse energy of 0.8 μJ. Under these conditions, the resulting craters exhibit diameters of approximately 750 nm with a center-to-center spacing of about 3.5 μm. Increasing the pulse energy to 1.2 μJ produces the array shown in Figure 2(b). At this higher energy, the ablation sites expand significantly; to accommodate the expansion, the approximate spacing between adjacent features was kept at 4.5 μm. The resulting craters showed diameters of approximately approaching 2 μm. Surface structure between craters is notably different from the original, indicating potential graphitization.

The altered surface texture between craters observed in Figure 2(b) is attributed to partial sp^3-to-sp^2 phase transformation, commonly referred to as laser-induced graphitization. Recent studies indicate that under femtosecond irradiation near the ablation threshold, this conversion is confined to a nanoscale surface layer-typically tens to approximately 100 nm in depth—and retains predominantly sp^3 character with localized sp^2 domains [34, 35]. At the fluences employed in the present work, the graphitized layer is expected to be superficial and should not significantly affect the mechanical or chemical properties relevant to microfluidic or field-emission applications. However, for electronic or photonic applications that depend on pristine diamond surface properties, post-processing steps such as oxidative etching may be employed to selectively remove the sp^2 phase without damaging the underlying sp^3 lattice [36].

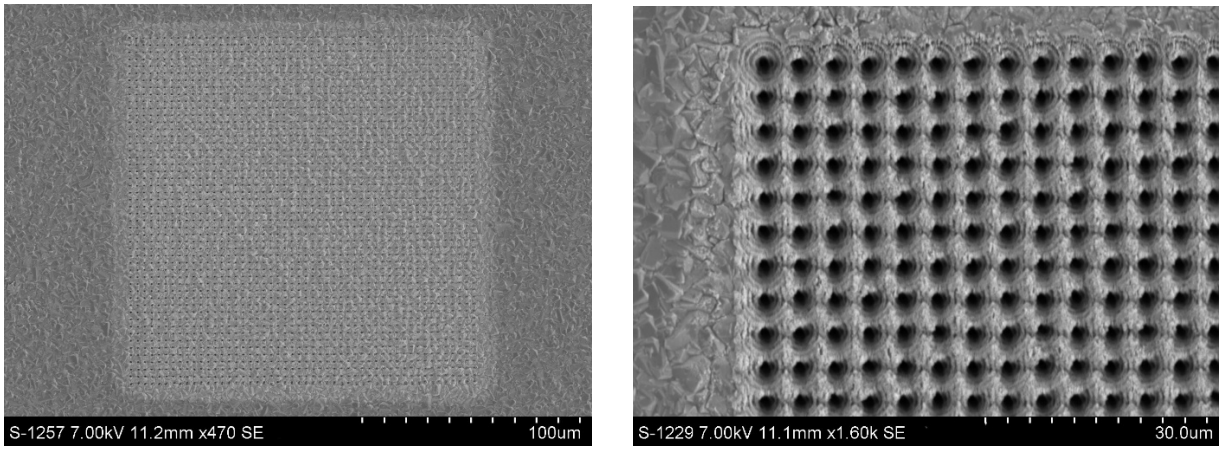

(a) (b)

Figure 2. SEM scans of laser-machined CVD diamond surface at laser pulse repetition rate of 250 kHz: (a) Laser Pulse Energy = 0.8 μJ; (b) Laser Pulse Energy = 1.2 μJ.

We next examine the effects of crater spacing on CVD diamond surface. In Figure 3, two patterns were machined a laser pulse energy of 1.2 μJ. The spacing between consecutive sites is approximately 3 μm for Figure 3(a) and 2.5 μm for Figure 3(b). The resulting patterns indicate that higher laser pulse energies and smaller hole spacing lead to feature overlap and form a continuous pattern.

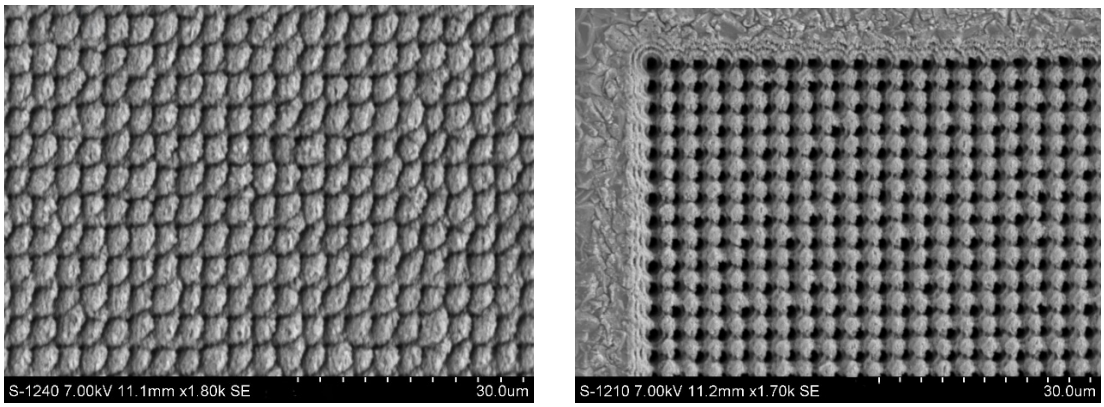

(a) (b)

Figure 3. SEM scans of laser-machined CVD diamond surface at laser pulse repetition rate of 250 kHz and Laser Pulse Energy of 1.2 μJ: (a) Pattern spacing = 3 μm; (b) Pattern spacing = 2.5 μm.

The observed increase in feature diameter and overlap with increasing pulse energy reflects the strong dependence of femtosecond laser ablation on deposited fluence. As the laser fluence exceeds the material ablation threshold, the radial region within the focal spot where the deposited energy surpasses the threshold expands, resulting in a corresponding increase in crater diameter. This behavior is consistent with the logarithmic scaling of ablation diameter with laser fluence observed in ultrafast micromachining of dielectric materials [2, 4]. In addition, higher pulse energies generate denser plasma within the focal volume, leading to enhanced energy coupling and increased material removal. These effects collectively contribute to the expansion and eventual overlap of adjacent ablation sites, enabling the formation of continuous surface structures.

Following the laser patterning, the surface features were replicated to investigate the depth and structure of machined features. Figure 4 shows an array of nanowires replicated from a corresponding array of craters ablated on CVD diamond surface. The original array was produced using a laser pulse energy of 2.2 μJ with a spatial separation of 10 μm between ablation sites. The SEM images of replicated arrays were taken at 45 degree tilt for a better estimate of feature depth. The height of acetate replica nanowires indicates that the craters in the original array reached a depth of approximately 6 μm.

The features of desired configurations can be fabricated by translating the sample through the focused laser beam incident on the surface. As mentioned above, arrays of holes or continuous patterns are produced through the controlled overlap of individual ablation sites. It is also possible to create other types of surface such as microchannels or reservoir. Channels are formed by delivering multiple consecutive laser pulses along a single path, resulting in continuous, well-defined structures. Figure 5 shows a microchannel fabricated on the surface of the CVD diamond at laser pulse energy of 0.8 μJ (a), and 2.2 μJ (b). The edges of the channel are well-defined, with minimal debris, and its width ranges between 1-2 μm.

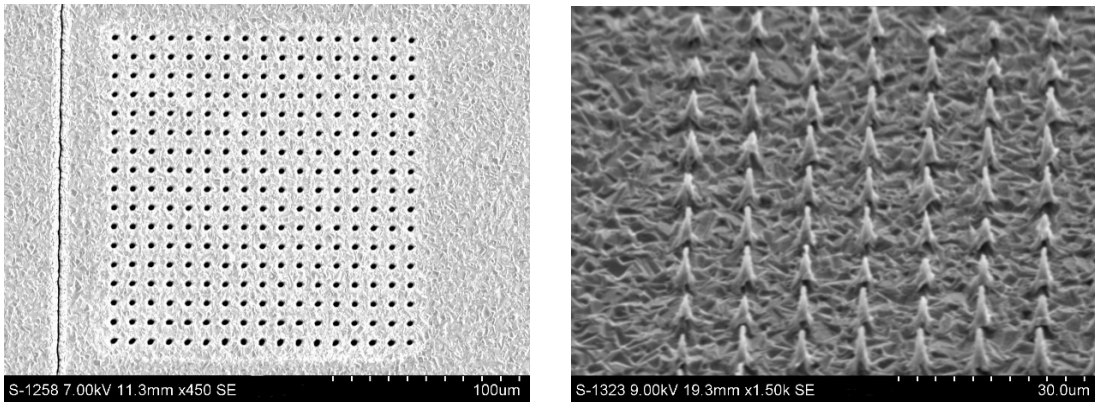

(a) (b)

Figure 4. CVD Diamond. (a) Surface machined at E=2.2 μJ, and (b) Replica of the surface (45 degree tilt).

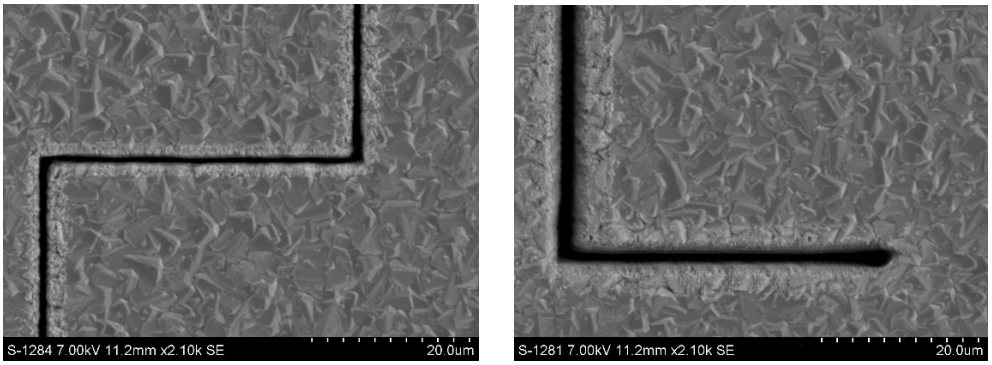

(a) (b)

Figure 5. Microchannel machined on CVD diamond surface at (a) E=0.8 μJ, and (b) E=2.2 μJ, with pulse repetition rate of 250 kHz.

Figure 6 shows a pattern of multiple vertical lines ablated on CVD diamond with a horizontal line spacing of approximately 4 μm and a feature width ranging from 0.8 to 1 μm. These structures were fabricated using a laser pulse energy of 1.8 μJ.

The observed feature widths of 0.8–1 μm exceed the diffraction-limited focal spot diameter of approximately 0.55 μm. This broadening is attributable to the extreme spatial pulse overlap achieved at the scanning speed of 11 μm/s and repetition rate of 250 kHz, corresponding to a pulse-to-pulse displacement of approximately 0.044 nm and an effective pulse overlap count on the order of ~12,500 pulses per spot diameter. Under these conditions, incubation effects progressively reduce the effective ablation threshold, allowing material removal to occur across a wider region of the Gaussian beam profile where the fluence exceeds the modified threshold. Additionally, the above-threshold area of the beam naturally extends beyond the $1/e^2$ spot radius at the pulse energy of 1.8 μJ employed. The combined effects of incubation-enhanced peripheral ablation and above-threshold fluence widening are consistent with established models of multipulse femtosecond laser machining [37, 38].

The variation of laser processing parameters allows fabrication of a wide range of structural designs with specific properties on the surface or in the bulk of a diamond. Careful selection of laser machining parameters produces well-defined microstructures, and is directed towards micromachining of fully-integrated assemblies, such as diamond emitters and fluidic devices. Figure 7 shows a reservoir structure on the CVD diamond surface. The reservoir was formed by translating the sample through the focused laser beam in a pre-programmed square pattern at a laser pulse energy of 3 μJ. The length of the sides of the feature is about 40 μm and the depth is approximately 8.8 μm.

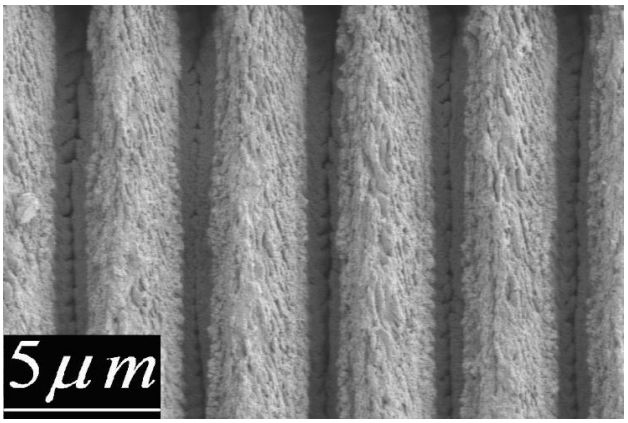

Figure 6. An array of microchannels on CVD diamond surface machined at E=1.8 μJ.

The formation of surface features on single-crystal diamond is examined next. Figure 8 shows an array of craters machined at the laser pulse energy of 0.8 μJ and repetition rate of 250 kHz on the surface of single-crystal diamond, and its acetate surface replica with the length of nanowires of approximately 5-7. This length is achieved at considerable lower laser pulse energies than in CVD diamond (Fig. 4).

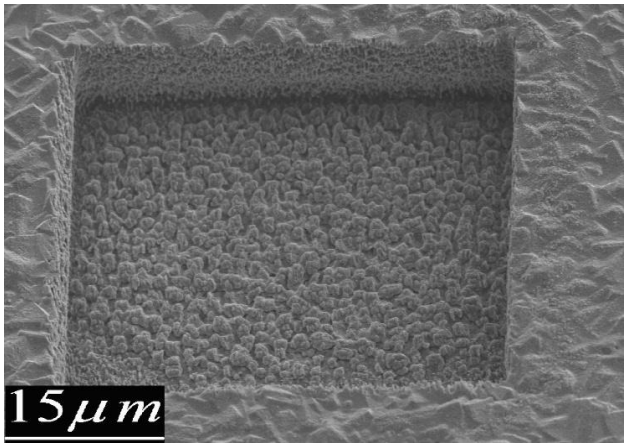

Figure 7. A reservoir structure on CVD diamond surface machined at E=3 μJ.

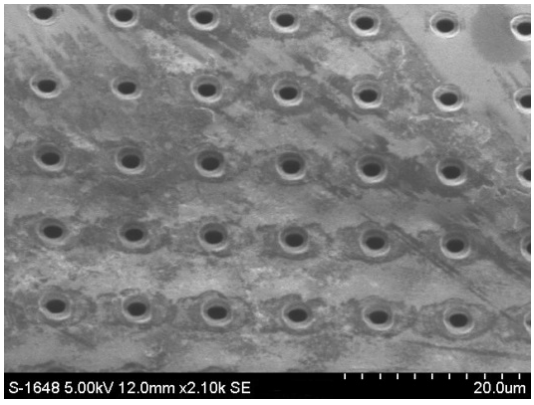

(a)

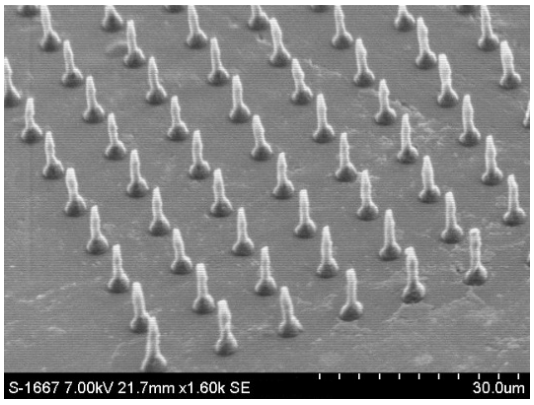

(b)

Figure 8. Single-Crystal Diamond surface. (a) Machined with incident energy of 0.8 μJ per pulse and repetition rate of 250 kHz, and (b) Array of nanowires from surface replication by acetate film.

Various surface features can be machined by translating a nanostage with a mounted sample through the focused laser beam. With the goal of device fabrication, we generated a curved pattern with sharp edges. The structure shown in Figure 9(a) was machined on HPHT single crystal diamond at laser pulse energy of 0.8 μJ, producing features with an estimated depth of 16-19 μm. This is considerably higher than the depth of features of 12-13 μm, observed for CVD diamond at similar laser pulse energies (Fig. 9(b)). The resulting structure exhibits well-defined morphology and shows that the process enables fabrication of curved features with high repeatability and spatial precision. SEM images were taken at 45-degree tilt for depth estimation.

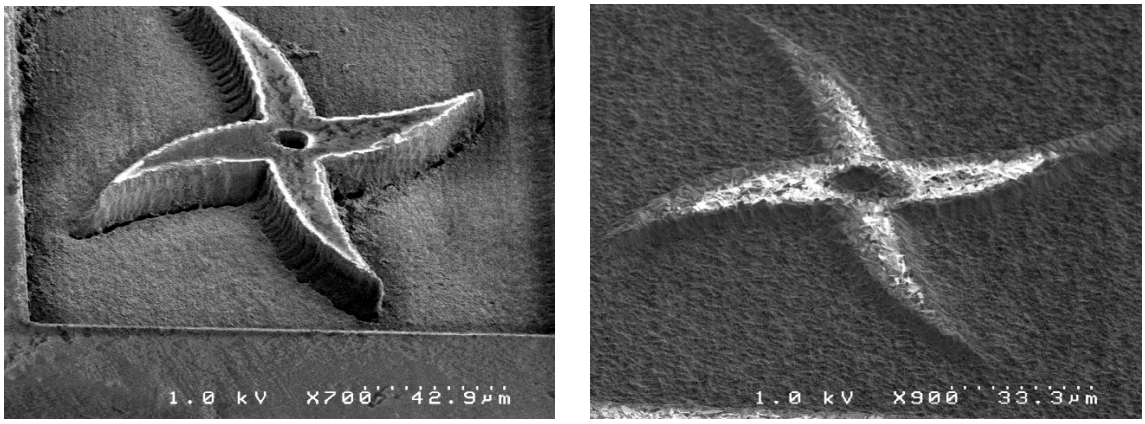

(a) (b)

Figure 9. A curved structure machined on the diamond surface at E= 0.8 µJ.
(a) HPHT Single Crystal Diamond, and (b) CVD Diamond.

The plasma dynamics underlying femtosecond laser ablation of wide-bandgap materials proceed through several distinct stages. During the laser pulse, nonlinear photoionization–including multiphoton ionization and tunneling ionization–generates seed free electrons in the conduction band. These electrons gain kinetic energy from the laser field through inverse bremsstrahlung absorption and, once they exceed the ionization energy of the lattice, trigger avalanche ionization that exponentially multiplies the free electron density. Within hundreds of femtoseconds, this process produces a dense, transient electron plasma confined to the focal volume. Following the termination of the laser pulse, the electron plasma transfers its energy to the lattice on a picosecond timescale through electron-phonon coupling. At fluences above the ablation threshold, two primary material removal mechanisms may contribute: Coulomb explosion, in which rapid electron ejection leaves behind a positively charged surface layer that undergoes electrostatic disintegration, and phase explosion, in which rapid lattice superheating drives explosive decomposition of the material into a mixture of vapor and nanoscale fragments [39, 40]. The subsequent expansion of the ablation plume carries ejected material away from the surface, leaving behind a well-defined crater. In single-crystal diamond, the highly ordered sp^3 lattice supports efficient avalanche ionization and dense plasma buildup, leading to strong energy confinement and rapid, directional plume expansion. In polycrystalline CVD diamond, grain boundaries and sp^2-rich intergranular regions act as carrier recombination centers and scattering sites, attenuating the buildup of the electron plasma and reducing the efficiency of energy coupling into the lattice. This results in lower ablation rates and less sharply defined features compared to single-crystal material [29, 41].

The features produced on single-crystal diamond are consistently deeper and exhibit sharper morphology than those generated on polycrystalline diamond under comparable irradiation conditions. This behavior arises from fundamental differences in the microstructure and electronic defect density of the two materials. Single-crystal diamond consists of a highly ordered sp^3-bonded lattice with minimal grain boundaries or impurity phases. In contrast, polycrystalline CVD diamond films typically contain grain boundaries, structural defects, and regions of graphitic or amorphous carbon. These features can act as carrier recombination centers and scattering sites that reduce the efficiency of avalanche ionization and limit the buildup of the electron plasma responsible for material removal. In single-crystal diamond, however, plasma expansion and reduced defect-mediated energy dissipation, as compared to polycrystalline material, contributes to increased ablation efficiency and improved feature quality. These findings further explain the deeper and more well-defined structures observed in single-crystal diamond [41].

The differences in bonding uniformity, defect density, and nonlinear ionization pathways lead to distinct ablation mechanisms in single-crystal and polycrystalline diamond. These material-dependent interaction processes directly influence feature morphology, depth, and reproducibility during femtosecond laser micromachining.

4. Conclusion

This work demonstrates that femtosecond laser ablation at 800 nm and 250 kHz repetition rate enables precise, non-thermal microstructuring of both HPHT single-crystal diamond and polycrystalline CVD diamond films, producing well-defined craters, microchannels, and reservoir structures. Both CVD and single-crystal diamond exhibit a strong dependence of ablation behavior on laser pulse energy; however, significant differences in feature size, depth, and morphology were observed between the two materials. Single-crystal diamond consistently produced deeper and more well-defined structures, reflecting differences in nonlinear absorption mechanisms, defect density, and plasma dynamics. These findings are consistent with recent reports demonstrating that ultrafast laser–diamond interactions are strongly influenced by crystal structure and impurity content.

Surface graphitization observed between ablation sites at higher pulse energies is confined to a nanoscale surface layer and does not compromise the structural integrity of the fabricated features for microfluidic or field-emission applications. Feature broadening beyond the diffraction-limited focal spot results from extreme pulse overlap and incubation-driven threshold reduction, offering a controllable mechanism for tuning channel width through scanning speed adjustment.

These results show that femtosecond laser micromachining is a viable single-step fabrication method for diamond-based microfluidic devices, field-emission structures, and photonic components, with material selection between single-crystal and polycrystalline diamond providing an additional degree of control over feature geometry and surface quality.

Acknowledgements

The authors acknowledge the support of the Center for Laser Applications at the University of Tennessee Space Institute.

Conflicts of interest

The authors declare no conflict of interest.

References

1. A. Zoubir et al., “Practical uses of femtosecond laser micro-materials processing,” *Appl. Phys. A*, vol. 77, pp. 311–315, 2003. https://doi.org/10.1007/s00339-003-2121-9

2. X. Liu, D. Du, and G. Mourou, “Laser ablation and micromachining with ultrashort laser pulses,” *IEEE J. Quantum Electron*., vol. 33, no. 10, pp. 1706–1716, 1997. https://doi.org/10.1109/3.631270

3. D. F. Farson et al., “Femtosecond laser micromachining of dielectric materials for biomedical applications,” *J. Micromech. Microeng*., vol. 18, no. 3, Art. no. 035020, 2008. https://doi.org/10.1088/0960-1317/18/3/035020

4. R. R. Gattass and E. Mazur, “Femtosecond laser micromachining in transparent materials,” *Nat. Photonics*, vol. 2, no. 4, pp. 219–225, 2008. https://doi.org/10.1038/nphoton.2008.47

5. A. Y. Kharin and V. Y. Timoshenko, “Optical properties of dextran-stabilized silicon nanoparticles in aqueous medium,” *Phys. Sci. Technol*., vol. 8, no. 3–4, pp. 22–27, 2021. https://doi.org/10.26577/phst.2021.v8.i2.03

6. A. Belarouci, R. Tkach, and D. Averin, “Engineering high aspect-ratio silicon nanostructures,” *Phys. Sci. Technol*., vol. 10, no. 3–4, pp. 87–94, 2023. https://doi.org/10.26577/phst.2023.v10.i2.011

7. A. M. Perelomov, V. S. Popov, and M. V. Terentev, “Ionization of atoms in an alternating electric field,” *Sov. Phys. JETP*, vol. 23, no. 5, pp. 924–934, 1966.

8. V. R. Bhardwaj, P. P. Rajeev, P. B. Corkum, and D. M. Rayner, “Strong field ionization inside transparent solids,” *J. Phys. B: At. Mol. Opt. Phys*., vol. 39, p. S397, 2006. https://doi.org/10.1088/0953-4075/39/13/S13

9. T. Abdulkareem Khalil Al-Aish and H. Amjed Kamil, “A new system to the spectroscopy analysis with multiple X-ray of free electron laser,” *Phys. Sci. Technol*., vol. 11, no. 3–4, pp. 86–91, 2024. https://doi.org/10.26577/phst2024v11i2b010

10. E. G. Gamaly, A. V. Rode, B. Luther-Davies, and V. T. Tikhonchuk, “Ablation of solids by femtosecond lasers: Ablation mechanism and ablation thresholds for metals and dielectrics,” *Phys. Plasmas*, vol. 9, no. 3, pp. 949–957, 2002. https://doi.org/10.1063/1.1447555

11. A. S. Saidov, S. N. Usmonov, and U. K. Rakhmonov, “Diamond films obtained on silicone substrates by the CVD method and properties of structures based on them,” *Phys. Sci. Technol*., vol. 10, no. 1–2, pp. 35–41, 2023. https://doi.org/10.26577/phst.2023.v10.i1.05

12. K. E. Spear and J. P. Dismukes, Eds., *Synthetic diamond: Emerging CVD science and technology*. New York, NY, USA: Wiley, 1994.

13. T. Kononenko, M. Meier, M. Komlenok, et al., “Microstructuring of diamond bulk by IR femtosecond laser pulses,” *Appl. Phys. A* 90, 645–651, 2008. https://doi.org/10.1007/s00339-007-4350-9

14. Y.-L. Liou et al., “Fabrication and field emission properties of ultra-nanocrystalline diamond lateral emitters,” *Diamond Relat. Mater*., vol. 17, no. 4–5, pp. 776–781, 2008. https://doi.org/10.1016/j.diamond.2008.01.024

15. K. Subramanian et al., “Nanodiamond lateral field emitter devices on thick insulator substrates for reliable high-power applications,” *Diamond Relat. Mater*., vol. 17, no. 4–5, pp. 786–789, 2008. https://doi.org/10.1016/j.diamond.2007.10.026

16. P. S. Salter and M. J. Booth, "Ultrafast laser processing of diamond," in *Proc. SPIE*, vol. 8974, 2014, Art. no. 89740T. https://doi.org/10.1117/12.2040384

17. A. Courvoisier, M. J. Booth, and P. S. Salter, "Inscription of 3D waveguides in diamond using an ultrafast laser," *Appl. Phys. Lett*., vol. 109, no. 3, 2016, Art. no. 031109. https://doi.org/10.1063/1.4959267

18. Y. V. White, X. Li, Z. Sikorski, L. M. Davis, and W. Hofmeister, "Single-pulse ultrafast-laser machining of high aspect nanoholes at the surface of SiO2," *Opt. Express*, vol. 16, no. 19, pp. 14411–14420, 2008. https://doi.org/10.1364/OE.16.014411

19. Y. V. White, M. Parrish, X. Li, L. M. Davis, and W. Hofmeister, "Femtosecond micro- and nano-machining of materials for microfluidic applications," in *Proc. SPIE*, vol. 7039, 2008, Art. no. 70390J. https://doi.org/10.1117/12.799855

20. W. P. Kang et al., "Diamond vacuum field emission devices," *Diamond Relat. Mater*., vol. 13, no. 11–12, pp. 1944–1948, 2004. https://doi.org/10.1016/j.diamond.2004.07.024

21. K. Subramanian et al., "Enhanced electron field emission from micropatterned pyramidal diamond tips incorporating CH4/H2/N2 plasma-deposited nanodiamond," *Diamond Relat. Mater*., vol. 15, no. 4–8, pp. 1126–1131, 2006. https://doi.org/10.1016/j.diamond.2005.12.047

22. Z. Rutkuniene, M. Balandyte, and G. Karbauskyte, "Formation of diamond-like carbon films on materials for medical application," *Phys. Sci. Technol*., vol. 8, no. 1–2, pp. 35–40, 2021. https://doi.org/10.26577/phst.2021.v8.i1.04

23. K. C. Phillips, H. H. Gandhi, E. Mazur, and S. K. Sundaram, "Ultrafast laser processing of materials: A review," *Adv. Opt. Photon*., vol. 7, pp. 684–712, 2015. https://doi.org/10.1364/AOP.7.000684

24. Y. Gurbuz et al., "PECVD diamond-based high performance power diodes," *IEEE Trans. Power Electron*., vol. 20, no. 1, pp. 1–10, 2005. https://doi.org/10.1109/TPEL.2004.839883

25. T. Apostolova, V. Kurylo, and G. Gnilitskyi, "Ultrafast laser processing of diamond materials: a review," *Front. Phys*., vol. 9, 2021, Art. no. 650280. https://doi.org/10.3389/fphy.2021.650280

26. V.V. Kononenko, "Modification of diamond surface by femtosecond laser pulses," *Photonics*, vol. 10, no. 10, 2023, Art. no. 1077. https://doi.org/10.3390/photonics10101077

27. A. Abdelmalek et al., "Morphological study of nanostructures induced by direct femtosecond laser ablation on diamond," *Micromachines*, vol. 12, p. 583, 2021. https://doi.org/10.3390/mi12050583

28. B. Khan, I. Litvinyuk, and M. Rybachuk, "Femtosecond laser micromachining of diamond: Current research status, applications and challenges," arXiv, 2021. https://doi.org/10.48550/arXiv.2103.00491

29. P. Calvani et al., "Absorptance enhancement in fs-laser-treated CVD diamond," *Phys. Status Solidi* A, vol. 212, pp. 2463–2467, 2015. https://doi.org/10.1002/pssa.201532189

30. O. Monteiro, "Structural defects and sp2 localization in CVD diamond," *J. Mater. Sci*., vol. 54, Art. no. 10, 2019. https://doi.org/10.1007/s10853-018-2949-1

31. M. Tulej et al., "Current progress in femtosecond laser ablation/ionisation time-of-flight mass spectrometry," *Appl. Sci*., vol. 11, no. 6, 2021, Art. no. 2562. https://doi.org/10.3390/app11062562

32. Y. Yao, H. Chen, and W. Zhang, "Time scale effects in laser material removal: A review," *Int. J. Adv. Manuf. Technol*., vol. 26, pp. 598–608, 2005. https://doi.org/10.1007/s00170-003-2026-y

33. X. Jing et al., "Modeling validity of femtosecond laser breakdown in wide bandgap dielectrics," *Appl. Surf. Sci*., vol. 258, no. 10, pp. 4741–4749, 2012. https://doi.org/10.1016/j.apsusc.2012.01.070

34. A. A. Khomich et al., "Raman study of the diamond to graphite transition induced by the single femtosecond laser pulse on the (111) face," *Nanomaterials*, vol. 13, no. 1, Art. no. 162, 2023. https://doi.org/10.3390/nano13010162

35. B. Ali et al., "Laser-induced graphitization of diamond under 30 fs laser pulse irradiation," J. *Phys. Chem. Lett*., vol. 13, pp. 2679–2685, 2022. https://doi.org/10.1021/acs.jpclett.2c00254

36. D. Zhang et al., "Structural evolution of polycrystalline diamond films under single-pulse femtosecond laser irradiation," *Appl. Surf. Sci*., vol. 702, 2025, Art. no. 163318. https://doi.org/10.1016/j.apsusc.2025.163318

37. G. Schnell, U. Duenow, and H. Seitz, "Effect of laser pulse overlap and scanning line overlap on femtosecond laser-structured Ti6Al4V surfaces," *Materials*, vol. 13, no. 4, p. 969, 2020. https://doi.org/10.3390/ma13040969

38. Z. Lin and M. Hong, "Femtosecond laser precision engineering: From micron, submicron, to nanoscale," *Ultrafast Sci*., vol. 2021, 2021, Art. no. 9783514. https://doi.org/10.34133/2021/9783514

39. S. A. Irimiciuc, P.-E. Nica, M. Agop, and C. Focsa, "Target properties – Plasma dynamics relationship in laser ablation of metals," *Appl. Surf. Sci*., vol. 506, 2020, Art. no. 144926. https://doi.org/10.1016/j.apsusc.2019.144926

40. J. Yao et al., "Exploring femtosecond laser ablation by snapshot ultrafast imaging and molecular dynamics simulation," *Ultrafast Sci*., vol. 2022, 2022, Art. no. 9754131. https://doi.org/10.34133/2022/9754131

41. J. Yin, G. Chen, Z. Zhu, M. Jin, and B. Hu, "Ablation mechanism investigation and ablation threshold prediction of single crystal diamond irradiated by femtosecond laser," *Diamond Relat. Mater*., vol. 111, 2021, Art. no. 108173. https://doi.org/10.1016/j.diamond.2020.108173

Information about the author:

Yelena V. White (corresponding author) – Doctor of Physics, Professor, Department of Biochemistry, Chemistry and Physics, Georgia Southern University (Swainsboro, USA, e-mail: ywhite@georgiasouthern.edu).